NANO LETTERS
Cite This: Nano Lett. XXXX, XXX, XXX−XXX
Letter
pubs.acs.org/NanoLett

Dual-Emitting Dot-in-Bulk CdSe/CdS Nanocrystals with Highly Emissive Core- and Shell-Based Trions Sharing the Same Resident Electron

Valerio Pinchetti,*[,†] Elena V. Shornikova,[‡] Gang Qiang,[‡] Wan Ki Bae,[§] Francesco Meinardi,[†] Scott A. Crooker,[∥] Dmitri R. Yakovlev,[‡,⊥] Manfred Bayer,[‡,⊥] Victor I. Klimov,*[,§] and Sergio Brovelli*[,†]

[†]Dipartimento di Scienza dei Materiali, Università degli Studi di Milano-Bicocca, via Roberto Cozzi 55, I-20125 Milano, Italy
[‡]Experimentelle Physik 2, Technische Universität Dortmund, 44227 Dortmund, Germany
[§]Chemistry Division, Los Alamos National Laboratory, Los Alamos, New Mexico 87545, United States
[∥]National High Magnetic Field Laboratory, Los Alamos National Laboratory, Los Alamos, New Mexico 87545, United States
[⊥]Ioffe Institute, Russian Academy of Sciences, 194021 St. Petersburg, Russia

Supporting Information

ABSTRACT: Colloidal CdSe nanocrystals (NCs) overcoated with an ultrathick CdS shell, also known as dot-in-bulk (DiB) structures, can support two types of excitons, one of which is core-localized and the other, shell-localized. In the case of weak "sub-single-exciton" pumping, emission alternates between the core- and shell-related channels, which leads to two-color light. This property makes these structures uniquely suited for a variety of photonic applications as well as ideal model systems for realizing complex excitonic quasi-particles that do not occur in conventional core/shell NCs. Here, we show that the DiB design can enable an unusual regime in which the same long-lived resident electron can endow trionlike characteristics to either of the two excitons of the DiB NC (core- or shell-based). These two spectrally distinct trion states are apparent in the measured photoluminescence (PL) and spin dynamics of core and shell excitons conducted over a wide range of temperatures and applied magnetic fields. Low-temperature PL measurements indicate that core- and shell-based trions are characterized by a nearly ideal (~100%) emission quantum yield, suggesting the strong suppression of Auger recombination for both types of excitations. Polarization-resolved PL experiments in magnetic fields of up to 60 T reveal that the core- and the shell-localized trions exhibit remarkably similar spin dynamics, which in both cases are controlled by spin-flip processes involving a heavy hole.

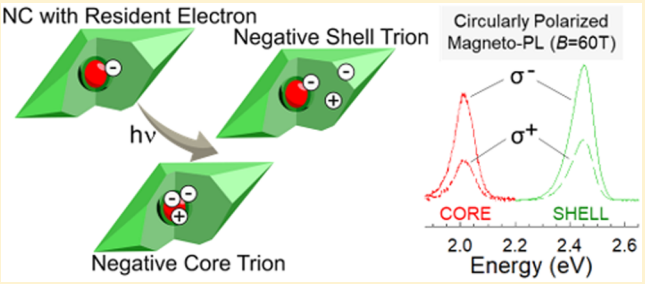

KEYWORDS: *Nanocrystals, core/shell heterostructures, dual emission, spin dynamics, charged excitons/trions*

Colloidal semiconductor nanocrystals (NCs) are solution-processed nanomaterials with high technological potential in solid-state lighting,[1−5] solar energy conversion,[6−9] bioimaging,[10−12] spintronics,[13−16] and sensing.[1,17] Over the years, tremendous progress in colloidal chemistry in combination with a greatly improved understanding of key photophysical features of the NCs has enabled the development of advanced multicomponent heterostructures that exhibit blinking-free photoluminescence (PL),[18,19] suppressed Auger recombination,[20,21] nearly 100% emission quantum yields,[22] and the capability of emitting two-color PL resulting from the radiative recombination of excitons localized in different compositional domains of the same NC.[23−28] Two-color light can be produced, in particular, by so-called dot-in-bulk NCs (DiB NCs) consisting of a small quantum-confined CdSe core embedded in an ultrathick bulklike CdS shell. These systems feature dual-color emission under both weak continuous wave (cw) optical[29] and electrical[30] excitation owing to a sharp interlayer of CdS in a zinc blende (ZB) phase separating the ZB CdSe core from the thick outer wurtzite (WZ) CdS shell (Figure 1a).[31] This peculiar polytypic shell structure reduces the rate of relaxation of photoholes from the thick CdS shell into the CdSe core and, together with electrostatic hole−hole repulsion, limits the occupancy of valence-band core states to just one hole.[29] This leads to an apparent violation of Kasha's rule,[32] as manifested in the coexistence of two distinct emission channels associated with core- and shell-localized excitons. Specifically, the core exciton has donorlike character and comprises an electron orbiting within the Coulomb potential of the core-localized hole,

Received: September 6, 2019
Revised: October 24, 2019
Published: October 25, 2019

DOI: 10.1021/acs.nanolett.9b03676
Nano Lett. XXXX, XXX, XXX−XXX

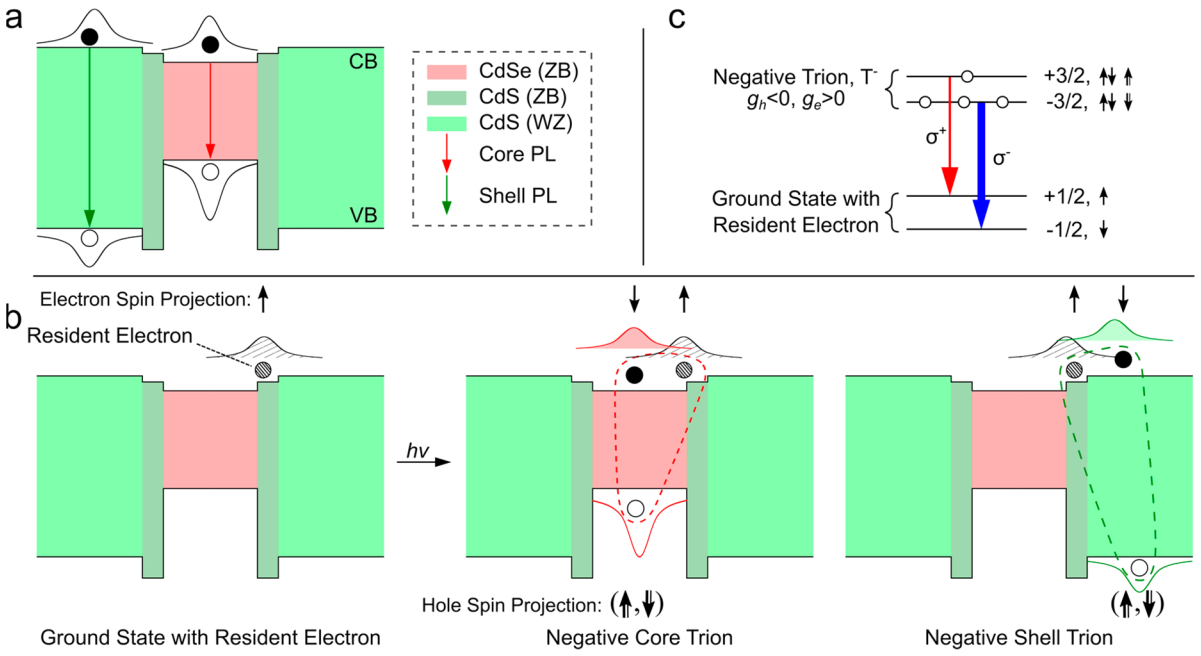

Figure 1. (a) Energy band diagram of a DiB NC featuring a CdSe core with the zinc blende (ZB) structure (red) overcoated with an epitaxial layer of CdS in the ZB phase (dark green), followed by a thick shell of CdS with the wurtzite (WZ) structure (light green). The core and shell excitons are also depicted. (b) Schematics of the formation of negative trions in the CdSe core (middle) and the CdS shell (right) upon photoexcitation of a negatively charged DiB NC (left). The core (shell) trions consist of the core (shell) exciton interacting with the resident electron (pattern filling). Because after thermalization the resident electron and the photoelectron occupy the same quantized state at the conduction band edge, the spin state of the photoelectron is dictated by the spin projection of the resident electron (assumed here to be a spin-up state), which is a direct consequence of the Pauli exclusion principle. The photohole can, in principle, reside in either of the spin states (up or down). (c) Schematic representation of the spin-level structures and the optical transitions for a negative trion comprising a heavy hole in a magnetic field. Double- and single-line short black arrows indicate hole and electron spins, respectively. Circularly polarized optical transitions are shown by red (σ^+) and blue (σ^-) arrows. The more intense emission, shown by the thicker blue arrow, originates from the lower-energy trion state with spin −3/2.

similar to conventional core-emitting thick-shell CdSe/CdS NCs. The shell exciton, on the other hand, is delocalized over the shell region and is somewhat similar to a coulombically bound exciton state of bulk CdS (if the CdSe core is unoccupied) or a bulklike exciton bound to a neutral donor (if the CdSe core is occupied with a single exciton).[29] Owing to the different exposure to the particle surfaces, the sensitivities of the core- and shell-emission channels of DiB NCs to the local chemical and/or electrochemical environments[30] are markedly different, which has been exploited in ratiometric probes of oxygen pressure[17] and intracellular pH in living human cells,[33] and in the context of artificial retina applications.[34]

In addition to their high potential for practical applications as single-particle multicolor emitters and ratiometric sensors, the ability of DiB NCs to host carriers in both the core and the shell regions opens exciting opportunities for realizing complex excitonic quasi-particles that cannot be observed with a conventional core/shell design. In particular, as we demonstrate here, the tendency of thick-shell CdSe/CdS NCs to photocharge (especially in vacuum and at low, cryogenic temperatures)[21,35] can be used to introduce a long-lived resident electron into a NC and then to study its interactions with excitons generated by photoexcitation. Because of a small conduction-band energy offset at the CdSe/CdS interface, the resident electron is delocalized across the entire NC and, as a result, is capable of efficiently interacting with both core- and shell-localized excitons. Specifically, as depicted in Figure 1b, photoexcitation of a charged DiB NC with a single electron–hole pair can, in principle, lead to the unique situation in which two different negative trions (T^-) can be alternately enabled by the same resident electron (Figure 1b, left). One trion can be realized because of the association of the long-lived electron with the core exciton (Figure 1b, middle), and the other, because of its interaction with the shell exciton (Figure 1b, right).

Presently, there is the consensus that, upon optical excitation, conventional (i.e., core-only-emitting) thick-shell CdSe/CdS NCs can be easily photoionized, which leaves the NC in a negatively charged state[21,35] that persists over long times, particularly in the absence of electron-withdrawing agents (such as oxygen)[21] or "oxidizing" electrochemical potentials.[36] Because of slow rates of charge neutralization, these NCs can be effectively considered to be "permanently" occupied by an additional resident electron, and their photoexcitation leads to the formation of T^- consisting of one hole and two opposite-spin electrons residing in the band-edge quantized state mostly localized in the CdSe core. Complete suppression of Auger recombination enabled by the thick-shell design leads to the nearly ideal (~100%) emission quantum yields of such core T^- states at cryogenic temperatures.[21] This is in contrast to the typically low PL efficiencies observed for T^- in core-only CdSe NCs wherein charged excitons quickly decay because of very fast nonradiative Auger recombination via the so-called negative trion pathway.[37]

The presence of permanent electrons is expected to dramatically modify optical and magneto-optical properties of negatively charged CdSe/CdS NCs with respect to neutral particles. The ground-state negative trion in these NCs is formed by two band-edge electrons and a band-edge heavy

DOI: 10.1021/acs.nanolett.9b03676
Nano Lett. XXXX, XXX, XXX−XXX

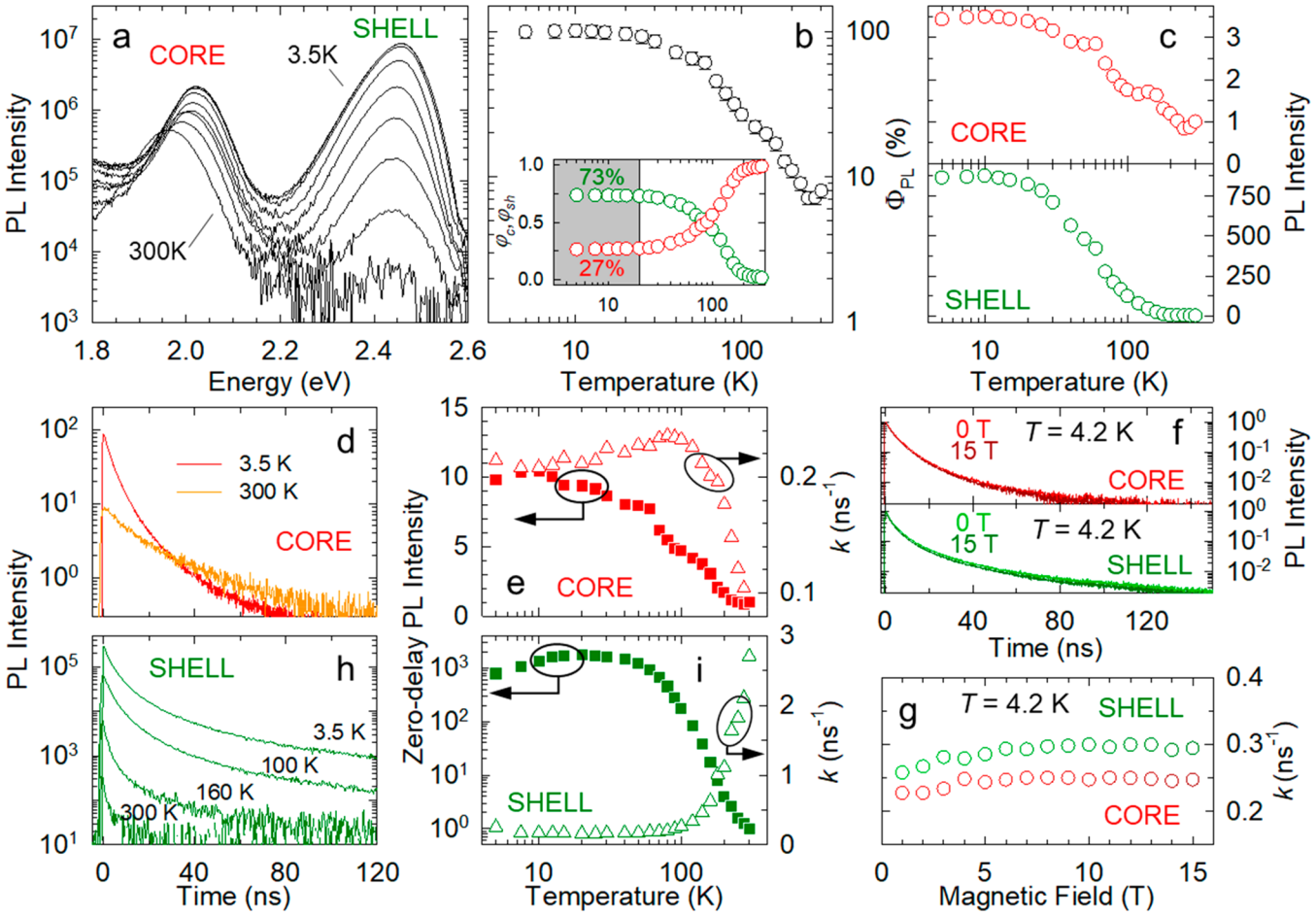

Figure 2. (a) PL spectra of CdSe/CdS DiB NCs (core radius 1.5 nm, shell thickness 8.5 nm) as a function of decreasing temperature from 300 to 3.5 K. (b) Total PL quantum yield (Φ_{PL}) and (inset) the relative weights of the core (φ_c) and the shell (φ_{sh}) PL as a function of temperature. In the low-temperature regime (T < 20 K, highlighted in gray), φ_c and φ_{sh} correspond to the probability of exciting the core- and shell-based excitons, respectively. (c) Spectrally integrated core and shell PL intensities (upper and lower panels, respectively) as a function of temperature normalized to their respective values at T = 300 K. (d) Core PL decay traces at T = 300 and 3.5 K (orange and red lines, respectively). (e) Zero-delay core PL intensities (solid red squares) and decay rates (open red triangles) as a function of temperature. (f) Normalized decays of the core (top panel, collected at 2.1 eV) and shell (bottom panel, collected at 2.45 eV) at T = 4.2 K and B = 0 and 15 T. (g) B dependence of the decay rate for the core (red circles) and the shell (green circles) luminescence extracted from the decay traces in Figure S3. (h) Shell PL decays at various temperatures and (i) temperature-dependent zero-delay shell PL intensities (solid green squares) and recombination rates (open green triangles). All measurements were performed using 3.06 eV pulsed excitation with a fluence of 10 nJ/cm^2, which corresponds to sub-single-exciton NC occupancies when the average number of electron−hole pairs generated per NC per pulse is much less than unity.

hole. Because the spins of the two electrons are oppositely aligned (Figure 1c), the total T^- angular momentum (J_T) is defined by the spin of the heavy hole, hence the J_T projections are equal to $M_T = \pm 3/2$. Both of these spin states are optically active; therefore, negative trions do not have a low-energy spin-forbidden "dark" state typical of neutral excitons. As a result, the low-temperature PL lifetime is orders of magnitude shorter than that of neutral excitons, and the T^- radiative decay rate is independent of the applied magnetic field (B).[38] These features are in contrast to the behaviors observed for neutral excitons for which magnetic-field-induced mixing of "dark" and "bright" states results in dramatic changes in the PL lifetime as a function of B.[39]

Another important feature of negative trions is that their spin dynamics are governed solely by the spin relaxation of heavy holes.[21,35,40] Because the final state following the radiative recombination of a T^- is a conduction band electron, the optical selection rule for the angular momentum projection ($\Delta M_T = \pm 1$) allows only the $+3/2 \rightarrow +1/2$ and $-3/2 \rightarrow -1/2$ transitions (Figure 1c). Because of the conservation of the total angular momentum, these transitions are coupled to photons with a specific handedness: clockwise (σ^+) and counterclockwise (σ^-), respectively.[35,38] As a result, an applied magnetic field splits the emission spectrum into a spin Kramer doublet composed of two oppositely circularly polarized bands with the photon helicity (clockwise or counterclockwise) determined solely by the spin projection of the heavy hole.

In this work, we show for the first time that a resident electron introduced into a CdSe/CdS DiB NC as a result of photocharging is capable of interacting with both core- and shell-localized excitons imparting trionlike characteristics to core and shell emission bands. In particular, circular polarization (CP)-resolved cw and time-resolved magneto-optical measurements reveal remarkably similar behaviors typical of negative trions for both core- and shell-localized carriers. Crucially, temperature (T)-dependent PL studies indicate that at T < 20 K both the core and shell trions decay primarily

DOI: 10.1021/acs.nanolett.9b03676
Nano Lett. XXXX, XXX, XXX−XXX

radiatively, suggesting the strong suppression of Auger decay for both species. Furthermore, we observe that the two T^- states feature very similar spin-flip rates that scale quadratically with the magnetic field.[35] As in previous studies of core-emitting CdSe/CdS NCs with a thinner shell,[35] this suggests that hole spin relaxation in our DiB NCs is mediated by a two-phonon process.

TEMPERATURE-DEPENDENT PHOTOLUMINESCENCE

The CdSe/CdS DiB NCs with a 1.5 nm core radius and a 8.5 nm shell thickness were synthesized following the route described in the Methods section.[29] As was observed previously for these NCs,[29,31,41] the X-ray diffraction patterns are dominated by the CdS shell with a WZ crystal structure (Figure S1). Transmission electron microscopy (TEM) images in Figure S2 show nonspherical particles, again in agreement with previous reports.[29,41,42]

We first investigate the effect of temperature on the two-color emission from the synthesized CdSe/CdS DiB NCs (Figure 2a). At T = 300 K, the PL spectrum is dominated by the core emission that peaks at 1.9 eV. The PL quantum yield (Φ_{PL}) is 8 ± 2% as measured with an integrating sphere. When the sample temperature is lowered from 300 to 3.5 K, both the core and the shell PL intensities grow significantly, so as the overall quantum yield is increased ca. 12-fold at $T \approx 20$ K, reaching >95% values (Figure 2b). This indicates that at T = 20 K and below, the core- and the shell-based states decay primarily radiatively.

A closer examination of the core PL (Figure 2c, top panel), indicates a progressive increase in the emission intensity with decreasing T, which saturates at around a 3.5-fold enhancement at T = 20 K. This behavior is similar to that of core-emitting thick-shell CdSe/CdS NCs that become negatively charged at low temperatures and exhibit a nearly unity T^- PL quantum yield below 10 K.[21] Time-resolved measurements of the core PL shown in Figure 2d indicate that charging of the CdSe core also occurs in DiB NCs. Specifically, we observe that as the temperature is reduced, the dynamics of neutral excitons turn into those of trions (Figure 2d,e). Three clear signatures of charging are the acceleration of the decay rate (k_T), which becomes approximately twice the neutral exciton rate (k_X), as expected for trions; the enhancement of the early-time PL amplitude;[36,37] and the lack of the dependence of the decay dynamics on applied magnetic fields.[35,38] In particular, our measurements indicate that the core PL decay rate (quantified in terms of the inverse of the time for which the PL signal drops by a factor of e) doubles from $k_{core,X}$ = 0.1 ns^{-1} at room temperature to $k_{core,T}$ = 0.2 ns^{-1} at $T \approx 20$ K and then stays nearly constant down to 3.5 K. Because at T < 20 K the PL quantum yield is close to unity, the 0.2 ns^{-1} rate can be attributed to the radiative decay of the core trion; the corresponding radiative lifetime is 5 ns. The increase in the PL decay rate with decreasing temperature is accompanied by the concomitant growth of the early-time PL amplitude (Figure 2e). However, instead of a 2-fold increase expected for the transition from the neutral exciton to trion emission,[43] the observed enhancement is approximately 10-fold. This suggests that at higher temperatures (T > 20 K) trion decay is contributed by a very fast nonradiative process (e.g., carrier trapping at interfacial defects), which is not resolved in our measurements. Apparently, this process gets suppressed with decreasing temperature so that at T < 20 K trion decay becomes primarily radiative.

As a confirmation of the formation of core trions at low temperatures, the core PL dynamics measured at T = 4.2 K is found to be independent of magnetic field up to B = 15 T (Figure 2f,g and Figure S3). As we indicated earlier, this behavior is expected for radiative recombination of the T^- species that do not have a "dark" state whose recombination would be forbidden due to angular momentum conservation.[35,38,39,44,45]

In contrast to a fairly moderate increase in the core-emission intensity, shell emission exhibits a dramatic, ~900-fold enhancement with decreasing temperature (Figure 2c, bottom panel). This large difference in the PL enhancement factor between the shell and the core PL implies that thermally assisted nonradiative processes affect the shell excitons much more significantly than the core excitons, likely because of their stronger exposure to surface states.[30] The strong effect of temperature on the shell PL is also evident from decay traces in Figure 2h, which show very fast growth of the zero-delay PL amplitude with decreasing T. In particular, as temperature is lowered from 300 to 3.5 K, the early-time PL signal increases by nearly 3 orders of magnitude (Figure 2i). This is accompanied by the decrease in the effective PL decay rate, which changes from 2.7 ns^{-1} at 300 K to 0.25 ns^{-1} at 3.5 K (Figure 2i). This behavior suggests the existence of two main T-dependent PL quenching processes characterized by distinct time scales; one is comparable to than that of radiative decay of shell excitons, and the other is much shorter than the radiative time constant. In fact, the second of these processes is so fast that it is not resolved in our measurements having ~600 ps resolution. Alternatively, the lack of discernible dynamics for the faster process might imply that it is associated with the trapping of a "hot" unrelaxed carrier as was previously observed for "B-type" blinking in standard "giant" CdSe/CdS NCs.[43]

As in the case of core emission, the shell PL intensity and the lifetime saturate at $T \leq 20$ K. Because in this temperature range the emission quantum yield reaches nearly ideal >95% values, this implies that shell-exciton recombination becomes almost purely radiative. As we indicated earlier, in this temperature range the core emission quantum efficiency also reaches nearly ideal values. Therefore, the relative intensities of the core and shell PL bands measured at T < 20 K can be used to quantify the branching ratio between the core and shell emission channels or, in other words, the probabilities of exciting core versus shell excitons (φ_c and φ_{sh}, respectively). In particular, on the basis of the data in the inset of Figure 2b, φ_c = 27% and φ_{sh} = 73%.

Again, in close similarity with observations for core PL, the shell PL dynamics are not affected by magnetic fields of up to B = 15 T (Figure 2f, bottom panel; Figure 2g), indicating that they are not due to neutral excitons but rather are trionlike. This suggests that the resident electron is delocalized between the core and the shell regions of the NCs in such a way that it is able to impart trionlike behavior to both core- and shell-based excitons. We stress that the measurements of the core and shell PL reported here are performed at very low excitation fluences (~10 nJ cm^{-2}) corresponding to sub-single-exciton occupancy of an individual DiB NC. As a result, the observed coexistence of core and shell trions occurs only at the ensemble level, whereas the individual excited NC contains a single exciton whose location alternates between the core and the shell. Because of the coupling of these excitons to the same

DOI: 10.1021/acs.nanolett.9b03676
Nano Lett. XXXX, XXX, XXX−XXX

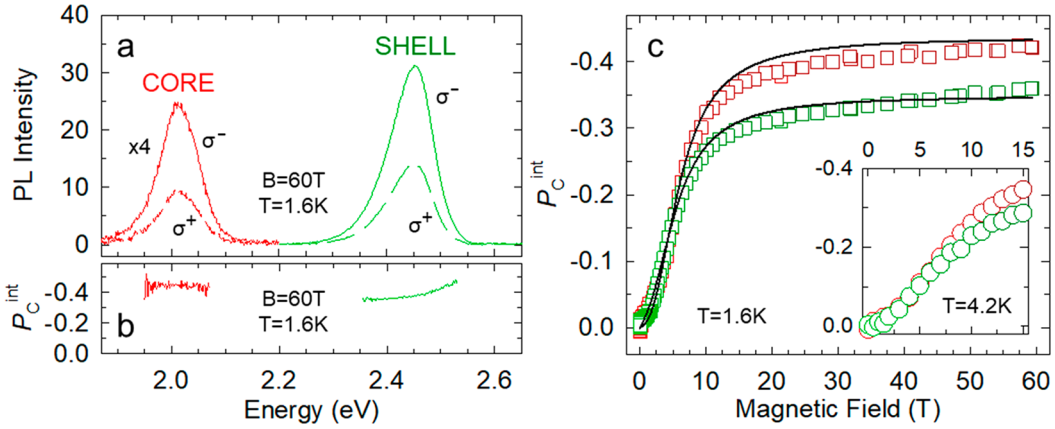

Figure 3. (a) Circular-polarization-resolved PL spectra of DiB NCs at T = 1.6 K and B = 60 T. The σ^- emission (continuous lines) is stronger than the σ^+ emission (dashed lines). (b) Respective P_c^{int} calculated using eq 1 as a function of emission energy. (c) Time-integrated P_c^{int} values for the core and shell PL (red and green squares, respectively) as a function of magnetic field up to B = 60 T measured at T = 1.6 K. The black lines are the P_c^{int} values modeled according to eq 7. Inset: Time-integrated P_c^{int} values for the core and the shell PL (red and green circles, respectively) as a function of magnetic field up to B = 15 T measured at T = 4.2 K.

resident electron they both exhibit trionlike characteristics. Interestingly, while strongly affecting radiative recombination dynamics and magneto-optical properties, the extra electron is Auger-decay-passive (i.e., it does not activate the negative trion Auger recombination pathway for either core- or shell-based excitons, at least at temperatures below 20 K).

TIME- AND CIRCULAR-POLARIZATION-RESOLVED MAGNETO-PHOTOLUMINESCENCE

Having assessed the temperature dependence of the core and shell luminescence, we proceed to the investigation of magneto-optical properties and spin dynamics of core- and shell-localized excitations. In particular, we measure the degree of circular polarization for the core and shell PL under an applied magnetic field of up to 60 T. In these measurements, we utilize a custom-built setup sketched in Figure S4. The sample was mounted on a fiber-coupled probe and loaded into a helium bath cryostat in a pulsed magnet. The sample was cooled to 1.6 K and excited by a 3.06 eV cw diode laser using low (sub-single-exciton) pump intensities. A thin-film circular polarizer was used to select the emitted light with circular polarization of only one handedness. To switch between the σ^+ and σ^- polarizations, we switched the direction of the pulsed current driving the magnet.

The CP-resolved PL data in Figure 3 show remarkably similar behaviors for the core and shell emission bands. For both of them, the σ^- component (I^-) is more intense than the σ^+ component (I^+), indicating that the g factor of the core-based excitations (g_{core}) is negative (Figure 3a). In CdSe NCs, the hole g factor is negative ($g_h < 0$)[35,45,46] and the electron g factor is positive ($g_e > 0$).[46,47] Therefore, the observation of $g_{core} < 0$, together with the low-temperature PL dynamics (Figure 2d,e) confirms the T^- origin of core-based excitations whose spin is solely determined by the angular momentum of the heavy hole (Figure 1c).[21,35] The similarity between the trends for the core and the shell CP-PL strongly suggests that the magneto-optical properties of the CdS shell are also dominated by the heavy hole, which is a result of the fact that, in a T^- electrons are in a singlet state and therefore have opposite spin orientation. In fact, as we show later, the g factor of shell-based excitations derived from spin-relaxation measurements is indeed close to that of bulk CdS heavy holes.

For a quantitative analysis of PL polarization properties, we introduce the degree of circular polarization, P_c, defined as follows

$$P_c = \frac{I^+(t, B, T) - I^-(t, B, T)}{I^+(t, B, T) + I^-(t, B, T)} \quad (1)$$

The spectral dependence of time-integrated P_c (denoted as P_c^{int}) of the core and the shell PL measured at T = 1.6 K and B = 60 T is reported in Figure 3b. Interestingly, P_c^{int} is nearly constant the core (~0.4−0.45) and shell (~0.35−0.4) spectral bands. Because different types of excitations are expected to have distinct spectroscopic and magneto-optical characteristics (such as spectral energies and g factors), this observation indicates that the core and shell bands are due to a single type of excitations (core- and shell-based trions, respectively) without an appreciable contribution from other species (e.g., neutral excitons).

The magnetic field dependences of core and shell P_c^{int} at T = 1.6 K are reported in Figure 3c (symbols) together with simulations (lines) according to the model described in detail later in this work. When B is increased, both core and shell P_c^{int} experience growth because of a progressive increase in the Zeeman splitting energy, ΔE_Z, between the two states of Kramer's doublets. The Zeeman splitting for negative trions[48] can be expressed as $\Delta E_Z = 3\mu_B|g_h|Bx$, where μ_B is the Bohr magneton. Multiplier x is equal to $\cos\beta$, where β is the angle between the direction of the magnetic field and the dipole moment (μ) of the optical transition. Similarly to plain CdSe NCs,[49] the P_c^{int} reaches near saturation levels for B > 15 T for both the core and the shell emission bands. The saturated value of P_c^{int} is ~0.4, which is lower than the intrinsic limit for a perfectly isotropic orientation of the dipoles (0.75).[49] This is likely due to partial alignment of the DiB NCs on the substrate surface as suggested by the relative intensities of the (100), (002) and (101) peaks in the XRD patterns (Figure S1), consistent with the preferred orientation along the (002) direction,[50] and by the TEM images in Figure S2. Previously, similar behavior was observed for densely packed films of CdSe/CdS colloidal nanoplatelets that showed a saturated P_c value of ~0.4 due to preferential alignment of the nanoplatelets with respect to the substrate.[48]

DOI: 10.1021/acs.nanolett.9b03676
Nano Lett. XXXX, XXX, XXX−XXX

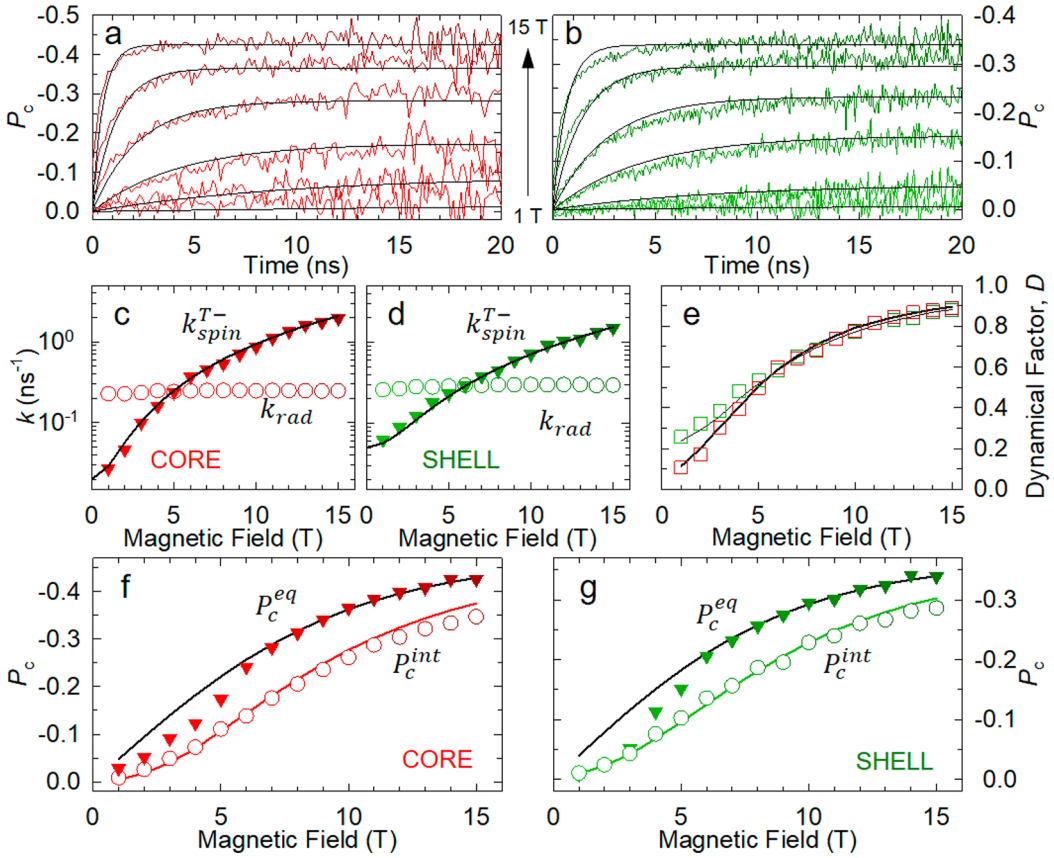

Figure 4. Time-resolved P_c at T = 4.2 K and B = 1, 3, 5, 7, 10, and 15 T for the (a) core and (b) shell emissions. B dependence of k_{spin}^{T-} (full triangles) and k_{rad} (open circles) for the (c) core and (d) shell. The black line is the fitting of k_{spin}^{T-} with eq 3. (e) Experimental (open symbols) and calculated (black lines) dynamical factors for the core (red) and shell (green) emission bands. (f) Core and (g) shell values of P_c^{int} (open circles) and P_c^{eq} (solid triangles) along with respective fits (black lines) obtained using eqs 5 and 7.

To study in greater detail the presaturation regime, we use a magneto-optical experiment which allows us to investigate temporal characteristics of CP-resolved PL using a 15 T superconducting magnet with a dc magnetic field (Figure S5). To confirm that the findings of dc B-field experiments can be used in conjunction with results of the pulsed-field measurements, we apply the dc-field configuration to analyze the B-dependent P_c^{int} (inset of Figure 3c). The results of these measurements are in close agreement with those of pulsed-field experiments, suggesting that the insights gained using one technique can be applied to interpreting the data obtained by the other.

By measuring polarized PL decay traces $I^+(t)$ and $I^-(t)$ as a function of the magnetic field and applying eq 1 (Figure S6), we obtain the transient polarization curves reported in Figure 4a,b (and Figure S7). As in the case of steady-state magneto-optical measurements discussed earlier, the time-resolved measurements of spin relaxation reveal surprising similarities in the behaviors of core- and shell-based excitations, which point once again to their similar identities. In particular, for both the core and the shell emissions, the recorded traces can be closely described by the empirical equation[35]

$$P_c(t, B, T) = P_c^{eq}(B, T)\{1 - \exp(-k_{spin}(B, T)t)\} \quad (2)$$

where $P_c^{eq}(B,T)$ is the equilibrium degree of circular polarization and $k_{spin}^{T-}(B, T)$ is the magnetic field- and temperature-dependent spin-flip rate for the core or for the shell excitations. Equation 2 captures the effects of both field amplitude and direction with respect to the dipole moment orientation. The application of a magnetic field parallel to μ (corresponding to x = 1) leads to a larger Zeeman splitting and, as a result, a larger P_c^{eq}. On the other hand, the perturbation induced by the perpendicular field (x = 0) leads to mixing between different spin states, which increases k_{spin}^{T-}.[35]

The latter effect is highlighted in Figure 4c,d, showing the spin-flip rates obtained by fitting the data in Figure 4a,b. For both the core and shell, k_{spin}^{T-} grows quadratically with B, and the trend can be well reproduced using the expression[35]

$$k_{spin}^{T-}(B, T) = k_{spin,0}^{T-} + \alpha(T)\, B^2(1 - x^2) \quad (3)$$

where $k_{spin,0}^{T-}$ is the spin relaxation rate in the absence of the applied magnetic field and the second term describes the B-field-induced spin relaxation (Table S1). Previously, a similar dependence was observed in ref 35 for trions in core-only emitting CdSe/CdS NCs, where the quadratic term was ascribed to a two-phonon relaxation mechanism. Apparently, a similar mechanism is operative in our DiB NCs, which controls the spin relaxation of both the core- and the shell-based trions. In particular, as expected for this mechanism, temperature-dependent, time-resolved CP-PL measurements reported in Figure S8 show the T^2 growth of k_{spin}^{T-} with temperature for both the core and shell trions. The spin-flip rate for shell-based trions has a stronger temperature dependence compared to that of the core T^-. This can be ascribed to the fact that the shell T^- state extends across the entire bulklike shell and therefore has a higher probability of interacting with phonons

DOI: 10.1021/acs.nanolett.9b03676
Nano Lett. XXXX, XXX, XXX−XXX

compared to core-based trions confined to a much smaller CdSe core.

It is instructive to compare the magnetic field dependence of the time-integrated polarization (P_c^{int}, Figure 3c) with the equilibrium values (P_c^{eq}) obtained under the same experimental conditions from the data in Figure 4a,b (derived by fitting to eq 2). For the purpose of this comparison, we use the dynamic factor, D, expressed as

$$D(T, B) = \frac{k_{spin}^{T-}(T, B)}{k_{spin}^{T-}(T, B) + k_{rad}(T, B)} \quad (4)$$

This factor yields the relative weight of the spin-flip rate with respect to the corresponding radiative recombination rate, k_{rad}. In other words, the dynamic factor quantifies the relative fraction of the PL decay that carries the maximum polarization possible for the given conditions (temperature and magnetic field) as defined by P_c^{eq}. The B dependence of both the core and shell dynamical factors is reported in Figure 4e. In both cases, D approaches unity, as expected for progressively faster spin-flip relaxation and a constant PL recombination rate.

Side-by-side plots of P_c^{int} and P_c^{eq} (Figure 4f,g) indicate that for both the core and shell PL bands $P_c^{int} < P_c^{eq}$ at any magnetic field. The observed difference between the two values is a direct consequence of $D < 1$ because at early times after excitation, when the PL is most intense, the emission is less circularly polarized because spin equilibrium is yet to be reached.

To extract the g factors of the core and shell T^-, we fit the experimental P_c^{eq} data with the equation[35]

$$P_c^{eq}(B, T, t) = -\frac{\int_i^f 2x\rho_0(B, x, T, t)\,dx}{\int_i^f (1 + x^2)\,dx} \quad (5)$$

where i and f define the range of NC-orientation-dependent x values and

$$\rho_0 = \tanh\left[\frac{\Delta E_Z}{k_B T}\right] \quad (6)$$

determines the relative populations of the spin sublevels in the state of equilibrium.

Similarly, the experimental P_c^{int} values can be fitted with the equation

$$P_c^{int}(B, T, t) = -\frac{\int_i^f 2x\rho_s(B, x, T, t)\,dx}{\int_i^f (1 + x^2)\,dx} \quad (7)$$

where $\rho_s = D\rho_0$.

In Figure 4f,g, we show the results of the fitting procedures using eqs 5 and 7; the corresponding sets of fitting parameters are reported in Table S2. Notably, the same parameters closely describe magneto-optical data acquired with B values that are as high as 60 T (Figure 3c). For the core T^-, the experimental data are reproduced using the hole g factor of −0.85, which is in good agreement with previous results obtained for CdSe nanostructures.[35,45,48] The magnetic field dependence of the shell P_c can be modeled using $g_h = -1.2$, in agreement with previous results for bulk CdS.[51−53] The discrepancy between the experimental data and the fitting curves at $B < 6$ T might be due to a magnetic field dependence of g_h, as was recently observed for two-dimensional CdSe/CdS nanoplateles.[48]

CONCLUSIONS

Our studies of magneto-optical properties of dual-emitting DiB NCs featuring a quantum-confined CdSe core embedded in a bulk-like polytypic CdS shell demonstrate that the presence of a persistent extra electron (introduced into an NC by spontaneous photocharging at low temperatures) enables an unusual photoexcitation regime where the same resident electron imparts trionlike behavior to both core- and shell-based excitons. The B-dependent measurements of low-temperature polarization-resolved PL and spin relaxation dynamics confirm the trionlike nature of core- and shell-based excitations. In particular, the analysis of PL polarization relaxation rates indicates that for both core and shell emission bands spin relaxation is controlled by the heavy hole spin-flip process, as expected for negative trions, wherein the two electron spins are oppositely aligned. Furthermore, the g factors derived from the B-dependent measurements of the degree of circular polarization for core ($g_{h,core} = -0.85$) and shell ($g_{h,shell} = -1.2$) emissions are consistent with those of heavy holes in CdSe and CdS, respectively. Importantly, at temperatures below 20 K, both types of trions show nearly ideal (>95%) emission efficiencies, indicating the strong suppression of nonradiative recombination via defect sites as well as greatly diminished rates of multicarrier Auger decay. The latter suggests that while having a strong effect on magneto-optical properties, the resident electron is Auger-recombination-passive, which is likely a result of the considerable spatial extent of the electron wave function delocalized between the core and shell regions of the DiB NC.

ASSOCIATED CONTENT

Supporting Information

The Supporting Information is available free of charge on the ACS Publications website at DOI: 10.1021/acs.nanolett.9b03676.

Methods, TEM images, XRD analysis, PL decay traces and CP-PL traces vs magnetic field and temperature, schematics of experimental setups, and fitting parameters (PDF)

AUTHOR INFORMATION

Corresponding Authors

*E-mail: valerio.pinchetti@unimib.it.
*E-mail: klimov@lanl.gov.
*E-mail: sergio.brovelli@unimib.it.

ORCID

Valerio Pinchetti: 0000-0003-3792-3661
Elena V. Shornikova: 0000-0002-6866-9013
Scott A. Crooker: 0000-0001-7553-4718
Dmitri R. Yakovlev: 0000-0001-7349-2745
Victor I. Klimov: 0000-0003-1158-3179
Sergio Brovelli: 0000-0002-5993-855X

Notes

The authors declare no competing financial interest.

ACKNOWLEDGMENTS

V.P., F.M., and S.B. thank the MIUR "Dipartimenti di Eccellenza 2017 Project − Materials for Energy". V.I.K. was supported by the Laboratory Directed Research and Development program of Los Alamos National Laboratory under project number 20200213DR. W.K.B. was supported by the

DOI: 10.1021/acs.nanolett.9b03676
Nano Lett. XXXX, XXX, XXX−XXX

Chemical Sciences, Biosciences and Geosciences Division, Office of Basic Energy Sciences, Office of Science, U.S. Department of Energy. Measurements at the NHMFL in Los Alamos were supported by the National Science Foundation (DMR-1644779) and the U.S. Department of Energy "Science of 100T" Program. E.V.S., G.Q., D.R.Y., and M.B. acknowledge the support of the Deutsche Forschungsgemeinschaft in the framework of ICRC TRR 160 (project B1).

REFERENCES

(1) Pietryga, J. M.; Park, Y.-S.; Lim, J.; Fidler, A. F.; Bae, W. K.; Brovelli, S.; Klimov, V. I. *Chem. Rev.* **2016**, *116* (18), 10513−10622.
(2) Dai, X.; Zhang, Z.; Jin, Y.; Niu, Y.; Cao, H.; Liang, X.; Chen, L.; Wang, J.; Peng, X. *Nature* **2014**, *515* (7525), 96−99.
(3) Mashford, B. S.; Stevenson, M.; Popovic, Z.; Hamilton, C.; Zhou, Z.; Breen, C.; Steckel, J.; Bulovic, V.; Bawendi, M.; Coe-Sullivan, S.; Kazlas, P. T. *Nat. Photonics* **2013**, *7* (5), 407−412.
(4) Castelli, A.; Meinardi, F.; Pasini, M.; Galeotti, F.; Pinchetti, V.; Lorenzon, M.; Manna, L.; Moreels, I.; Giovanella, U.; Brovelli, S. *Nano Lett.* **2015**, *15* (8), 5455−5464.
(5) Giovanella, U.; Pasini, M.; Lorenzon, M.; Galeotti, F.; Lucchi, C.; Meinardi, F.; Luzzati, S.; Dubertret, B.; Brovelli, S. *Nano Lett.* **2018**, *18* (6), 3441−3448.
(6) Carey, G. H.; Abdelhady, A. L.; Ning, Z.; Thon, S. M.; Bakr, O. M.; Sargent, E. H. *Chem. Rev.* **2015**, *115* (23), 12732−63.
(7) Meinardi, F.; Ehrenberg, S.; Dhamo, L.; Carulli, F.; Mauri, M.; Bruni, F.; Simonutti, R.; Kortshagen, U.; Brovelli, S. *Nat. Photonics* **2017**, *11* (3), 177−185.
(8) García de Arquer, F. P.; Armin, A.; Meredith, P.; Sargent, E. H. *Nat. Rev. Mater.* **2017**, *2*, 16100.
(9) Wu, K.; Li, H.; Klimov, V. I. *Nat. Photonics* **2018**, *12* (2), 105−110.
(10) Alivisatos, A. P.; Gu, W.; Larabell, C. *Annu. Rev. Biomed. Eng.* **2005**, *7*, 55−76.
(11) Kairdolf, B. A.; Smith, A. M.; Stokes, T. H.; Wang, M. D.; Young, A. N.; Nie, S. *Annu. Rev. Anal. Chem.* **2013**, *6*, 143−62.
(12) Dubertret, B.; Skourides, P.; Norris, D. J.; Noireaux, V.; Brivanlou, A. H.; Libchaber, A. *Science* **2002**, *298* (5599), 1759−1762.
(13) Pandey, A.; Brovelli, S.; Viswanatha, R.; Li, L.; Pietryga, J. M.; Klimov, V. I.; Crooker, S. A. *Nat. Nanotechnol.* **2012**, *7* (12), 792−797.
(14) Fainblat, R.; Barrows, C. J.; Hopmann, E.; Siebeneicher, S.; Vlaskin, V. A.; Gamelin, D. R.; Bacher, G. *Nano Lett.* **2016**, *16* (10), 6371−6377.
(15) Capitani, C.; Pinchetti, V.; Gariano, G.; Santiago-Gonzalez, B.; Santambrogio, C.; Campione, M.; Prato, M.; Brescia, R.; Camellini, A.; Bellato, F.; Carulli, F.; Anand, A.; Zavelani-Rossi, M.; Meinardi, F.; Crooker, S. A.; Brovelli, S. *Nano Lett.* **2019**, *19* (2), 1307−1317.
(16) Pinchetti, V.; Di, Q.; Lorenzon, M.; Camellini, A.; Fasoli, M.; Zavelani-Rossi, M.; Meinardi, F.; Zhang, J.; Crooker, S. A.; Brovelli, S. *Nat. Nanotechnol.* **2018**, *13* (2), 145−151.
(17) Lorenzon, M.; Pinchetti, V.; Bruni, F.; Bae, W. K.; Meinardi, F.; Klimov, V. I.; Brovelli, S. *Nano Lett.* **2017**, *17* (2), 1071−1081.
(18) Mahler, B.; Spinicelli, P.; Buil, S.; Quelin, X.; Hermier, J. P.; Dubertret, B. *Nat. Mater.* **2008**, *7* (8), 659−664.
(19) Chen, Y.; Vela, J.; Htoon, H.; Casson, J. L.; Werder, D. J.; Bussian, D. A.; Klimov, V. I.; Hollingsworth, J. A. *J. Am. Chem. Soc.* **2008**, *130* (15), 5026−5027.
(20) Lim, J.; Park, Y.-S.; Klimov, V. I. *Nat. Mater.* **2018**, *17*, 42.
(21) Javaux, C.; Mahler, B.; Dubertret, B.; Shabaev, A.; Rodina, A. V.; Efros, A. L.; Yakovlev, D. R.; Liu, F.; Bayer, M.; Camps, G.; Biadala, L.; Buil, S.; Quelin, X.; Hermier, J. P. *Nat. Nanotechnol.* **2013**, *8*, 206−212.
(22) Dai, X.; Zhang, Z.; Jin, Y.; Niu, Y.; Cao, H.; Liang, X.; Chen, L.; Wang, J.; Peng, X. *Nature* **2014**, *515*, 96.
(23) Soni, U.; Pal, A.; Singh, S.; Mittal, M.; Yadav, S.; Elangovan, R.; Sapra, S. *ACS Nano* **2014**, *8* (1), 113−123.
(24) Liu, S.; Borys, N. J.; Sapra, S.; Eychmüller, A.; Lupton, J. M. *ChemPhysChem* **2015**, *16* (8), 1663−1669.
(25) Battaglia, D.; Blackman, B.; Peng, X. *J. Am. Chem. Soc.* **2005**, *127* (31), 10889−10897.
(26) Sapra, S.; Mayilo, S.; Klar, T. A.; Rogach, A. L.; Feldmann, J. *Adv. Mater.* **2007**, *19* (4), 569−572.
(27) Zhao, H.; Sirigu, G.; Parisini, A.; Camellini, A.; Nicotra, G.; Rosei, F.; Morandi, V.; Zavelani-Rossi, M.; Vomiero, A. *Nanoscale* **2016**, *8*, 4217.
(28) Dias, E. A.; Grimes, A. F.; English, D. S.; Kambhampati, P. *J. Phys. Chem. C* **2008**, *112* (37), 14229−14232.
(29) Galland, C.; Brovelli, S.; Bae, W. K.; Padilha, L. A.; Meinardi, F.; Klimov, V. I. *Nano Lett.* **2013**, *13* (1), 321−328.
(30) Brovelli, S.; Bae, W. K.; Meinardi, F.; Santiago González, B.; Lorenzon, M.; Galland, C.; Klimov, V. I. *Nano Lett.* **2014**, *14* (7), 3855−3863.
(31) Pinchetti, V.; Meinardi, F.; Camellini, A.; Sirigu, G.; Christodoulou, S.; Bae, W. K.; De Donato, F.; Manna, L.; Zavelani-Rossi, M.; Moreels, I.; Klimov, V. I.; Brovelli, S. *ACS Nano* **2016**, *10* (7), 6877−6887.
(32) Lakowicz, J. R. *Principles of Fluorescence Spectroscopy*, 3rd ed.; Springer: 2006.
(33) Bruni, F.; Pedrini, J.; Bossio, C.; Santiago-Gonzalez, B.; Meinardi, F.; Bae, W. K.; Klimov, V. I.; Lanzani, G.; Brovelli, S. *Adv. Funct. Mater.* **2017**, *27* (12), 1605533.
(34) Mosconi, E.; Salvatori, P.; Saba, M. I.; Mattoni, A.; Bellani, S.; Bruni, F.; Santiago Gonzalez, B.; Antognazza, M. R.; Brovelli, S.; Lanzani, G.; Li, H.; Brédas, J.-L.; De Angelis, F. *ACS Energy Lett.* **2016**, *1* (2), 454−463.
(35) Liu, F.; Biadala, L.; Rodina, A. V.; Yakovlev, D. R.; Dunker, D.; Javaux, C.; Hermier, J.-P.; Efros, A. L.; Dubertret, B.; Bayer, M. *Phys. Rev. B: Condens. Matter Mater. Phys.* **2013**, *88* (3), 035302.
(36) Galland, C.; Ghosh, Y.; Steinbrück, A.; Hollingsworth, J. A.; Htoon, H.; Klimov, V. I. *Nat. Commun.* **2012**, *3*, 908.
(37) Jha, P. P.; Guyot-Sionnest, P. *ACS Nano* **2009**, *3* (4), 1011−1015.
(38) Shabaev, A.; Rodina, A. V.; Efros, A. L. *Phys. Rev. B: Condens. Matter Mater. Phys.* **2012**, *86* (20), 205311.
(39) Nirmal, M.; Norris, D. J.; Kuno, M.; Bawendi, M. G.; Efros, A. L.; Rosen, M. *Phys. Rev. Lett.* **1995**, *75* (20), 3728−3731.
(40) Christodoulou, S.; Vaccaro, G.; Pinchetti, V.; De Donato, F.; Grim, J. Q.; Casu, A.; Genovese, A.; Vicidomini, G.; Diaspro, A.; Brovelli, S.; Manna, L.; Moreels, I. *J. Mater. Chem. C* **2014**, *2* (17), 3439−3447.
(41) Brovelli, S.; Bae, W. K.; Galland, C.; Giovanella, U.; Meinardi, F.; Klimov, V. I. *Nano Lett.* **2014**, *14* (2), 486−494.
(42) Tan, R.; Yuan, Y.; Nagaoka, Y.; Eggert, D.; Wang, X.; Thota, S.; Guo, P.; Yang, H.; Zhao, J.; Chen, O. *Chem. Mater.* **2017**, *29* (9), 4097−4108.
(43) Galland, C.; Ghosh, Y.; Steinbrueck, A.; Sykora, M.; Hollingsworth, J. A.; Klimov, V. I.; Htoon, H. *Nature* **2011**, *479*, 203−207.
(44) Norris, D. J.; Efros, A. L.; Rosen, M.; Bawendi, M. G. *Phys. Rev. B: Condens. Matter Mater. Phys.* **1996**, *53* (24), 16347−16354.
(45) Efros, A. L.; Rosen, M.; Kuno, M.; Nirmal, M.; Norris, D. J.; Bawendi, M. *Phys. Rev. B: Condens. Matter Mater. Phys.* **1996**, *54* (7), 4843−4856.
(46) Gupta, J. A.; Awschalom, D. D.; Efros, A. L.; Rodina, A. V. *Phys. Rev. B: Condens. Matter Mater. Phys.* **2002**, *66* (12), 125307.
(47) Karimov, O. Z.; Wolverson, D.; Davies, J. J.; Stepanov, S. I.; Ruf, T.; Ivanov, S. V.; Sorokin, S. V.; O'Donnell, C. B.; Prior, K. A. *Phys. Rev. B: Condens. Matter Mater. Phys.* **2000**, *62* (24), 16582−16586.
(48) Shornikova, E. V.; Biadala, L.; Yakovlev, D. R.; Feng, D.; Sapega, V. F.; Flipo, N.; Golovatenko, A. A.; Semina, M. A.; Rodina, A. V.; Mitioglu, A. A.; Ballottin, M. V.; Christianen, P. C. M.; Kusrayev, Y. G.; Nasilowski, M.; Dubertret, B.; Bayer, M. *Nano Lett.* **2018**, *18* (1), 373−380.

DOI: 10.1021/acs.nanolett.9b03676
Nano Lett. XXXX, XXX, XXX−XXX

(49) Johnston-Halperin, E.; Awschalom, D. D.; Crooker, S. A.; Efros, A. L.; Rosen, M.; Peng, X.; Alivisatos, A. P. *Phys. Rev. B: Condens. Matter Mater. Phys.* **2001**, *63* (20), 205309.
(50) Holder, C. F.; Schaak, R. E. *ACS Nano* **2019**, *13* (7), 7359−7365.
(51) Hopfield, J. J.; Thomas, D. G. *Phys. Rev.* **1961**, *122* (1), 35−52.
(52) Venghaus, H.; Suga, S.; Cho, K. *Phys. Rev. B: Condens. Matter Mater. Phys.* **1977**, *16* (10), 4419−4428.
(53) Blattner, G.; Kurtze, G.; Schmieder, G.; Klingshirn, C. *Phys. Rev. B: Condens. Matter Mater. Phys.* **1982**, *25* (12), 7413−7427.

DOI: 10.1021/acs.nanolett.9b03676
Nano Lett. XXXX, XXX, XXX−XXX